HKUST Theoretical Computer Science Center Research Report HKUST-TCSC-98-10

Design and Analysis of Planar Shape Deformation *

Siu-Wing Cheng[†] Herbert Edelsbrunner[‡] Ping Fu[§] and Ka-Po Lam[†]

Abstract

Shape deformation refers to the continuous change of one geometric object to another. We develop a software tool for planning, analyzing, and visualizing deformations between two shapes in $\mathbb{R}^2$. The deformation is generated automatically without any user intervention or specification of feature correspondences. A unique property of the tool is the explicit availability of the two-dimensional shape space, which can be used for designing the deformation either automatically by following constraints and objectives or manually by drawing deformation paths.

1 Introduction

This paper describes a method for the deformation of one geometric shape in the plane to another and a software tool that implements it. In computer graphics this operation is commonly referred to as *morphing*. In that area the focus is on the creation of image sequences that *display* the morph [8, 9, 10]. In contrast, this paper constructs the deformation as a 1-dimensional family of genuine geometric objects.

Rationale. This paper follows the general ideas about shape representation and deformation laid out in [2, 3]. It focuses on the special case of *two* shapes in *two* dimensions. Even in this simplest of all interesting cases there is a frightening amount of freedom and an abundant variety of possible deformations. It has been suggested we follow the general trend of making up an evaluation function and compute the optimal deformation defined by that function. The authors of this paper believe that this strategy fails to rationalize the process as it only shifts the irrational decisions one level higher. Instead, we follow a path of deformation design that permits efficient quantitative analysis. The deformations satisfy basic requirements, such as economy in shape variation, local smoothness, and geometric integrity. Other than that the method employs natural geometric operations, such as lifting, taking convex hulls, slicing, and projecting. All constructions are global and mathematically defined. The full description of these constructions and higher-dimensional interpretations is beyond the scope of this paper and we refer the interested reader to [2].

The criticism of lacking an optimality criterion and the above response apply only to the automatic reconstruction of deformations. Section 4 explains how the system permits the specification of evaluation functions and the optimization within a 2-dimensional space of shapes.

Summary of results. The software tool described in this paper constructs and deforms 2-dimensional shapes and it rationalizes the process through analysis and visualization. Some of the features of that tool are now listed.

- The source and target shapes are regular sets in $\mathbb{R}^2$: each set is the closure of its interior. The sets can have arbitrarily many components and holes. The chosen data structure places no principle limitations on the kind of shapes although it is better in representing some types than others. The appearance of the shapes for small data sets is similar to the blobby models introduced by Blinn [1].
- The deformation can be computed fully automatically, which means that also the topology of the

*This research is partially supported by RGC CERG HKUST 190/95E and by NSF CCR-96-19542.

[†]Department of Computer Science, Hong Kong University of Science and Technology, Kowloon, Hong Kong.

[‡]Department of Computer Science, University of Illinois at Urbana-Champaign, and Raindrop Geomagic, Inc.

[§]Raindrop Geomagic, Inc., and National Computational Science Alliance, University of Illinois at Urbana-Champaign.

shape is changed without user intervention. See figure 1 for an example where a '0' with one hole is deformed into a '1' without hole.

- Each intermediate shape is determined by a time parameter, $t \in [0, 1]$, and a size parameter, $\alpha^2 \in \mathbb{R}$. In the automatic and unconstrained deformation the size is a function of t and the initial and final size values. Deformation paths satisfying shape constraints can be designed in the 2-dimensional shape space of time and size.
- The deformation is monitored by keeping track of quantitative information, such as the area, boundary length, number of components, and number of holes. Constraints guiding the automatic design of a deformation can be formulated in terms of these quantities.

The tool provides VCR functionalities for the interactive visualization, such as play, reverse, step forward, step backward, etc.

Ramifications. The widespread use of image morphing in the movie and advertisement industries justifies the related research, maybe also the one reported in this paper. The particular properties and features of the method described in this paper suggests additional applications.

- The shape is well defined at every moment during the deformation. If we stack up all 2-dimensional shapes we get a pipe-like 3-dimensional shape that smoothly starts, branches, joins, and ends. Such pipes are good models of blood vessels. Another example are complicated exhaust systems, and the constrained deformation option can be used to maintain, say, a constant cross-section area.
- The automatic deformation between two given shapes is canonical. The kind and amount of change can be used to define a distance measure between shapes useful for example in automatic pattern recognition. It might be worth trying out this idea in the classification of printed and possibly even handwritten Chinese characters.
- The shape space embedding the deformations is explicitly given as a 2-dimensional strip of pairs $(t, \alpha^2) \in [0, 1] \times \mathbb{R}$. If the source and target shapes are significantly different then this space is an index into a rich variety of shapes. This suggests applications in shape compression and the design of shape databases.

Figure 1: Read the pictures from left to right and top to bottom as a deformation from '0' to '1'.

Outline. Section 2 reviews the two basic ingredients to our deformation tool: the shape representation of [3] and the deformation technique of [2]. Section 3 explains the various geometric concepts used in the construction and visualized by the software tool. Section 4 discusses the structure of the shape space and how it is exploited in the design of special deformation paths. Section 5 concludes the paper.

2 Shape and Deformation

The full details of the shape representation and the shape deformation methods can be found in [3] and in [2]. This section explains the minimum of both formalisms and relies on illustrations to provide an intuition for the ideas. Every shape is represented by two data structures: a complex that captures structure and connectivity and a set with smooth boundary that serves as the appearance of the shape. We explain first the two data structures and second the deformation method.

Structure and connectivity. We begin by specifying the input data, which is a set of weighted points or disks, and the Voronoi decomposition of the plane this set defines. Each disk in the input set $B = \{b_1, b_2, \ldots, b_n\}$ is specified by its center and its radius: $b_i = (z_i, \varrho_i)$ with $z_i \in \mathbb{R}^2$ and ${\varrho_i}^2 \in \mathbb{R}$. We permit negative ${\varrho_i}^2$ which corresponds to an imaginary radius, ϱ_i, and an imaginary disk, b_i. The *(weighted) distance* of a point $x \in \mathbb{R}^2$ from b_i is $\pi_i(x) = \|x - z_i\|^2 - {\varrho_i}^2$, and the *(weighted) Voronoi cell* of b_i is the set of points no closer to any other disk:

$$V_i = \{x \in \mathbb{R}^2 \mid \pi_i(x) \leq \pi_j(x), \text{ for all } j\},$$

see figure 2. The Voronoi cells decompose the union of

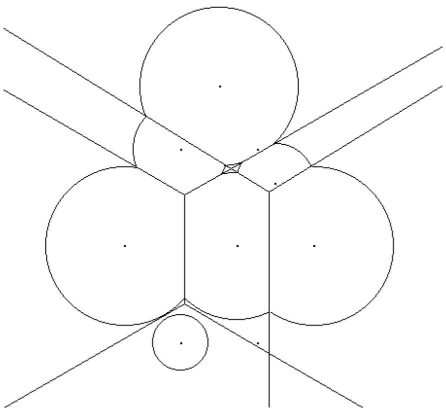

Figure 2: The Voronoi cells of 9 disks, 7 with positive and 2 with imaginary radius. Two of the centers do not lie in their Voronoi cells.

disks into convex cells: $\bigcup B = \bigcup_{i=1}^{n}(V_i \cap b_i)$. Any two of these cells are either disjoint or they meet along a portion of their boundaries.

The *complex* data structure is denoted as $\mathrm{Dsx}\, B$ and records the overlap between the cells $R_i = V_i \cap b_i$. Specifically, z_i is a vertex in $\mathrm{Dsx}\, B$ iff $R_i \neq \emptyset$ and $z_i z_j$ is an edge iff $R_i \cap R_j \neq \emptyset$. Furthermore, $\mathrm{conv}\,\{z_i \mid i \in I\}$ is a 2-dimensional cell, for I a set of three or more disk indices, iff $\bigcap_{i \in I} R_i \neq \emptyset$ and I is maximal with this property. For B in general position all cells in $\mathrm{Dsx}\, B$ are triangles. However, we cannot reasonably make this simplifying assumption because the deformation method described shortly systematically creates degenerate disk sets, such as the one shown in figure 2. Even if we have general position at times $t = 0$ and $t = 1$ there are parallelograms in the intermediate complexes, see figure 3.

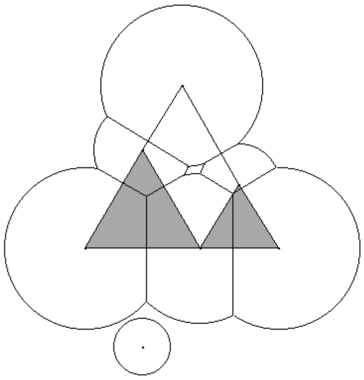

Figure 3: The Voronoi decomposition and complex of the union of disks in figure 2. The complex contains only two cells, namely the shaded triangles. The white parallelogram would belong to the complex, along with other cells, if the disks were larger.

Shape appearance. The body is defined as a union of an infinite family of disks, and the skin is its boundary, which is the envelope of an infinite family of circles. To define these families observe that $b_i = {\pi_i}^{-1}(-\infty, 0]$ and its bounding circle is ${\pi_i}^{-1}(0)$. The weighted distance functions span the usual vector space defined by function addition and scaling. Let $\Pi = \{\pi_i \mid 1 \leq i \leq n\}$ be the collection of weighted distance functions. The affine hull of Π is the family of combinations $\sum \gamma_i \cdot \pi_i$, where the γ_i add up to 1. The convex hull is the subfamily defined by non-negative scaling factors:

$$\mathrm{conv}\, \Pi = \{\sum_{i=1}^{n} \gamma_i \cdot \pi_i \mid \sum_{i=1}^{n} \gamma_i = 1, \gamma_i \geq 0 \text{ for all } i\}.$$

The convex hull is an infinite family of paraboloid functions and we construct the skin and body by shrinking each $\pi \in \mathrm{conv}\, \Pi$ using a parameter $0 \leq s \leq 1$. For $\pi(x) = \|x - z\|^2 - \varrho^2$ define the shrunken function as

$$\pi^s(x) = \frac{1}{s} \cdot \|x - z\|^2 - \varrho^2.$$

The zero-set of π^s is the circle with center z and radius $\sqrt{s}\varrho$. The envelope and union of the infinite family of shrunken disks is now defined with the help of the pointwise minimum function, $\Gamma_s(x) = \min\{\pi^s(x) \mid \pi \in$

conv $\Pi\}$:

$$\begin{aligned}\mathrm{skn}^s B &= \Gamma_s^{-1}(0),\\ \mathrm{bdy}^s B &= \Gamma_s^{-1}(-\infty, 0].\end{aligned}$$

They are referred to as the *s-skin* and the *s-body* of B, see figure 4.

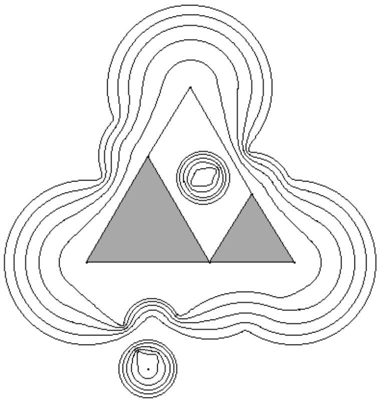

Figure 4: The skins for $s = 0.1, 0.3, 0.5, 0.7, 0.9$ of the same set of disks as in figures 2 and 3. Observe that the complex is contained in the five bodies and they are all connected the same way, with two components of which one has a hole and the other does not.

Shape deformation. Let B and C be two finite sets of disks defining the initial and the final shapes of the deformation. Intermediate shapes are constructed by interpolating between the two sets. It is convenient to project a cross-section of the vector space of weighted distance functions onto the set of disks. Formally, if b and c are disks with weighted distance functions π and φ and $\gamma_1 + \gamma_2 = 1$ then $a = \gamma_1 \cdot b + \gamma_2 \cdot c$ is the disk with weighted distance function $\gamma_1 \cdot \pi + \gamma_2 \cdot \varphi$. With this introduction define

$$\begin{aligned}A_t &= (1-t) \cdot B + t \cdot C\\ &= \{(1-t) \cdot b + t \cdot c \mid b \in B, c \in C\}\end{aligned}$$

for every $t \in [0, 1]$. Clearly $A_0 = B$ and $A_1 = C$. For a given value of s, we thus have a one-parameter family of shapes,

$$\mathbb{X}_t = \mathrm{bdy}^s A_t,$$

that deforms the initial shape, $\mathbb{X}_0 = \mathrm{bdy}^s B$, into the final shape, $\mathbb{X}_1 = \mathrm{bdy}^s C$, see figure 5.

Observe the automatic change of topology that happens synchronously for the skin and the complex. In figure 5 there is a change in topology between all contiguous snapshots except for the last three. Even though the seventh and the eight snapshot have the same topology, the latter is obtained from the former by two changes, one filling a hole and one opening a hole. The second, third, fourth, and sixth snapshots are taken right at the time of a topology change when two components or two portions of the same component reach each other in a point and locally separate the complement.

3 Visualization of Concepts

The display panel of the software tool can be used to visualize all geometric concepts mentioned in section 2 and more.

Basic structures. Let B be a finite set of disks as before. The *(weighted) Voronoi complex*, denoted as $\mathrm{Vor}\, B$, is the collection of 2-dimensional Voronoi cells together with common intersections among them. The *(weighted) Delaunay complex*, denoted as $\mathrm{Del}\, B$, records the overlap among 2-dimensional Voronoi cells, see the rightmost example in figure 6.

Next we discuss a nested sequence of subcomplexes of the Delaunay complex. Let $\alpha^2 \in \mathbb{R}$ and define $b_i(\alpha)$ as the disk with center z_i and radius $\sqrt{\varrho_i{}^2 + \alpha^2}$. We have $b_i(0) = b_i$, and if $\varrho_i{}^2 = 0$ then the radius of $b_i(\alpha)$ is α. Let $B(\alpha) = \{b_i(\alpha) \mid b_i \in B\}$ and observe that the Voronoi complex of $B(\alpha)$ is the same as that of B. In other words, the Voronoi complex and the Delaunay complex do not vary with α^2. The cells of the convex decomposition of $\bigcup B(\alpha)$ grow with α:

$$R_i(\alpha_1) = V_i \cap b_i(\alpha_1) \subseteq V_i \cap b_i(\alpha_2) = R_i(\alpha_2)$$

if $\alpha_1 \leq \alpha_2$. We call $\mathrm{Dsx}_\alpha B = \mathrm{Dsx}\, B(\alpha)$ the *α-complex* of B. The collection of such complexes is nested and the last one is the Delaunay complex:

$$\emptyset = \mathrm{Dsx}_{\alpha_0} B \subseteq \mathrm{Dsx}_{\alpha_1} B \subseteq \mathrm{Dsx}_{\alpha_2} B = \mathrm{Del}\, B,$$

where $\alpha_0^2 \leq \alpha_1^2 \leq \alpha_2^2$, α_0^2 is sufficiently small, and α_2^2 is sufficiently large, see figure 6.

Decomposed skin and body. Similar to the union of disk we can decompose the skin and the body into simple pieces. The complex that produces the decomposition consists of 2-dimensional Voronoi cells, 2-dimensional Delaunay cells, and rectangles that are

Cartesian products of matching Voronoi and Delaunay edges. All these cells are shrunk so they fit together to form a decomposition of $\mathbb{R}^2$. To describe this complex let $0 \leq s \leq 1$ be arbitrary but fixed. Let I be a subset of indices with

$$\begin{aligned} \nu_I &= \bigcap_{i \in I} V_i \in \operatorname{Vor} B, \\ \delta_I &= \operatorname{conv}\{z_i \mid i \in I\} \in \operatorname{Del} B. \end{aligned}$$

The dimension of ν_I is $k \in \{0, 1, 2\}$ and that of δ_I is $2 - k$. The corresponding (2-dimensional) cell in the complex is

$$\mu_I{}^s = s \cdot \nu_I + (1 - s) \cdot \delta_I,$$

where addition and scaling refer to the operations in the vector space of points in $\mathbb{R}^2$. The *s-mixed complex*, denoted as $\operatorname{Mix}^s B$, consist of all cells $\mu_I{}^s$ and all non-empty common intersections among them, see figure 7.

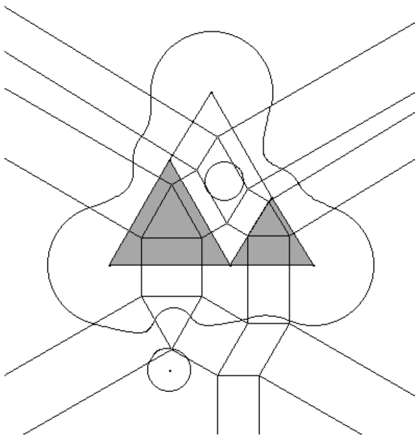

Figure 7: The 0.5-skin of the disk set in figure 2 is decomposed into circle and hyperbola arcs by the 0.5-mixed complex.

Observe that $\operatorname{Mix}^0 B = \operatorname{Del} B$ and $\operatorname{Mix}^1 B = \operatorname{Vor} B$. For all other values of s, $\operatorname{Mix}^s B$ contains a shrunken copy of every Voronoi and Delaunay cell. The copy of V_i intersects $\operatorname{skn}^s B$ in a collection of arcs that all belong to a common circle, namely the zero-set of $\pi_i{}^s$. Similarly, the copy of a Delaunay cell intersects the skin in a collection of arcs that all belong to a common circle, but this circle is not the boundary of any shrunken disk in B. This can be seen from the fact that the body lies outside every circle of the latter type. The remaining 2-dimensional cells in $\operatorname{Mix}^s B$ are rectangles, and each rectangle intersects the skin in a collection of arcs that belong to a common hyperbola. A more detailed description of the skin decomposition including formulas for all circles and hyperbolas can be found in [3].

Complementarity. We develop an explicit expression of the symmetry between shape and complement by introducing another set of disks. Call two disks $b_i = (z_i, \varrho_i)$ and $b_j^\perp = (y_j, \rho_j)$ *orthogonal* if

$$\|z_i - y_j\|^2 = \varrho_i{}^2 + \rho_j{}^2,$$

and *further than orthogonal* if the square distance between the centers exceeds the sum of square radii. In case of real radii the bounding circles of two orthogonal disks meet at right angles. We construct a new set of disks, $B^\perp = \{b_1^\perp, b_2^\perp, \ldots, b_m^\perp\}$, that cover the part of $\mathbb{R}^2$ outside $\bigcup B$ and overlap the disks in B orthogonally or less. Specifically, for each vertex y_j of $\operatorname{Vor} B$ choose the radius ρ_j so $b_j^\perp = (y_j, \rho_j)$ is orthogonal to all b_i with $y_j \in V_i$. By definition of Voronoi complex, $b_j^\perp$ is further than orthogonal from all other disks in B. For completeness, we stipulate a Voronoi vertex at infinity in the direction of each unbounded Voronoi edge and define the corresponding disk as a half-plane. It is not difficult to see that $\operatorname{Vor} B = \operatorname{Del} B^\perp$ and $\operatorname{Del} B = \operatorname{Vor} B^\perp$, and therefore $(B^\perp)^\perp = B$. Two additional noteworthy properties are:

$$\begin{aligned} \operatorname{bdy}^s B \cup \operatorname{bdy}^{1-s} B^\perp &= \mathbb{R}^2, \\ \operatorname{bdy}^s B \cap \operatorname{bdy}^{1-s} B^\perp &= \operatorname{skn}^s B = \operatorname{skn}^{1-s} B^\perp. \end{aligned}$$

Figure 8 illustrates the relationship between B and $B^\perp$ by showing three skins of B, for $s = 0, 0.5, 1$. The 0-body of B is the closed complement of a union of disks, namely the complement of the interior of $\bigcup B^\perp$. The 0.5-skin shrinks away from the boundaries of $\bigcup B$ and of $\bigcup B^\perp$ and lies between $\operatorname{skn}^0 B = \operatorname{skn}^1 B^\perp$ and $\operatorname{skn}^1 B = \operatorname{skn}^0 B^\perp$.

Deformation and topology change. We return to the deformation constructed by interpolating disk sets: $A_t = (1-t) \cdot B + t \cdot C$, see section 2. Let $0 < s < 1$ be fixed and let t vary inside $[0, 1]$ and generate a 1-parameter family of shapes, $\mathbb{X}_t = \operatorname{bdy}^s A_t$. We focus on the local picture of a change in topology as t varies continuously. Each change occurs at a particular moment in time and a particular point in the plane. Let this point be z and distinguish three cases depending on the type of cell in the mixed complex that contains z.

Case $I = \{i\}$. Point z lies inside the shrunken Voronoi cell $\mu_I{}^s$. The cell specifies the portion of the circle defined by b_i that belongs to the skin. This circle is

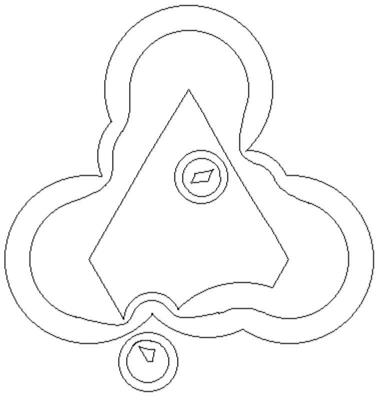

Figure 8: The boundary of $\bigcup B$, the boundary of $\bigcup B^\perp$, and the common 0.5-skin of B and $B^\perp$ separating the two boundaries.

the zero-set of ${\pi_i}^s$. In the non-degenerate case the radius of this circle is either imaginary or positive real. The topology change happens at the transition from the former case to the latter or vice versa. This transition either creates a new component by growing a disk from z or it removes a component by shrinking a disk to z.

CASE $I = \{i, j\}$. Point z lies inside the rectangle ${\mu_I}^s$. The rectangle specifies the portion of the hyperbola defined by b_i and b_j that belongs to the skin. The hyperbola consists of two branches living in diagonally opposite quadrants defined by the two asymptotic lines, see figure 9. In the non-degenerate case the two branches either locally separate or locally sandwich the body. The topology change happens at the transition when the hyperbola equals the two asymptotic lines and flips from on pair of opposite quadrants into the other. The transition either creates a bridge by locally joining two portions of the body at z, or it removes a bridge by locally separating two portions at z.

CASE $I = \{i, j, k\}$. Point z lies inside the shrunken Delaunay triangle ${\mu_I}^s$. In degenerate configurations I may contain more than three indices and ${\mu_I}^s$ may have more than three sides. The triangle specifies the portion of the circle defined by $b_\ell^\perp$ orthogonal to b_i, b_j, b_k that belongs to the skin. Observe the symmetry to card $I = 1$. The non-degenerate cases are again when the radius of the circle is either positive real or imaginary. The transition either removes a hole by shrinking a disk to z or it creates a hole by growing a disk from z.

Asymmetry of deformation. For a fixed $t \in [0, 1]$, $A_t = (1-t) \cdot B + t \cdot C$ is a set of disk and we consider its Voronoi and Delaunay complexes, see figure 10. Combinatorially, the Delaunay complex changes only twice, from $t = 0$ to $t \in (0, 1)$ to $t = 1$. Geometrically, it moves all the time as the cells gradually change shape. Interestingly, the situation is different for the Voronoi complex, and this in spite of the symmetry between the two complexes noted above. The Voronoi complexes of the A_t are the same for all $t \in (0, 1)$. Specifically, each such Voronoi complex is the overlay of $\mathrm{Vor}\, A_0$ and $\mathrm{Vor}\, A_1$, see again figure 10. The asymmetry is explained by the asymmetry of the deformation. An alternative definition of deformation uses the shapes defined by the complementary disk sets:

$$D_t^\perp = (1-t) \cdot B^\perp + t \cdot C^\perp.$$

$D_t^\perp$ is different from $A_t^\perp$ except at the beginning, at $t = 0$, and at the end, at $t = 1$. To see that the two are indeed different, in general, note that $(A_t^\perp)^\perp = A_t$. So when $A_t^\perp$ changes as t increases, the Voronoi complex changes and the Delaunay complex is invariant. On the other hand, when $D_t^\perp$ changes as t increases, the Delaunay complex changes and the Voronoi complex is invariant.

4 Deformation Design

The control panel of the software tool contains the VCR buttons that drive the deformation through the selection and alteration of time and size. The explicit representation of the 2-dimensional shape space permits the rational design of deformations.

Shape space. Let the two disk sets B and C define the initial and the final shape of a deformation problem. We have an intermediate shape defined for each value $t \in [0, 1]$ of the time parameter and each value $\alpha^2 \in \mathbb{R}$ of the size parameter. Specifically, the shape is defined by the set of disks $A_t(\alpha)$, where $A_t = (1-t) \cdot B + t \cdot C$. We use (t, α^2) as a coordinate pair to specify shapes in

$$\mathbf{\Omega} = [0, 1] \times \mathbb{R},$$

which we refer to as *shape* or *state space*. $\mathbf{\Omega}$ is a 2-dimensional strip that can be decomposed into regions within which the shape variation is insignificant. As an example consider the decomposition into shapes whose complexes are the same: $\mathbb{X}_1 = \mathrm{bdy}\, A_{t_1}(\alpha_1)$ and $\mathbb{X}_2 = \mathrm{bdy}\, A_{t_2}(\alpha_2)$ are *similar* if $\mathrm{Dsx}_{\alpha_1} A_{t_1} = \mathrm{Dsx}_{\alpha_2} A_{t_2}$.

Since the moments in time the two shapes exist are in general different this needs some clarification. Although the Delaunay complex moves with time, its combinatorial structure is the same during the entire open time interval. We therefore have an unambiguous notion of *sameness* for Delaunay cells over time and it makes sense to refer to a Delaunay cell δ_I without specifying the time, which can be anywhere in $(0,1)$. Two complexes at different moments in time are the *same* if they contain the same cells. Similarity among shapes is therefore well defined and it is an equivalent relation.

Curve arrangement. We gain insight into the decomposition of $\mathbf{\Omega}$ by considering a single Delaunay cell, δ_I. For each time $t \in (0,1)$ let $f_I(t)$ be the smallest real number so $\delta_I(t)$ belongs to $\mathrm{Dsx}_\alpha A_t$ iff $\alpha^2 \geq f_I(t)$. For each 2-dimensional δ_I the discriminating function is linear:

$$f_I(t) \quad = \quad a_1 \cdot t + a_0.$$

For Delaunay edges and vertices the description of f_I is made complicated by the somewhat technical distinction between attached and unattached cells, see e.g. [5]. A cell δ_I is *attached* at time t if for every $\alpha^2 \in \mathbb{R}$ the presence of $\delta_I(t)$ in $\mathrm{Dsx}_\alpha A_t$ implies the presence of a higher-dimensional cell, δ_J, that contains δ_I as a face. Since δ_J cannot be in the complex without its faces this implies $f_I(t) = f_J(t)$ for this value of t. The interesting case is when $\delta_I(t)$ is unattached. For example if δ_I is 2-dimensional then it is unattached during the entire open time interval. In general, δ_I is unattached during a single and possibly empty time interval. In that time interval the discriminating function is at most quadratic:

$$f_I(t) \quad = \quad a_2 \cdot t^2 + a_1 \cdot t + a_0,$$

with $a_2 \leq 0$. We picture $\mathbf{\Omega}$ and its decomposition by drawing time from left to right and size from bottom to top. The graphs of the discriminating functions are lines that pass through the strip from left to right and upside-down parabolas that begin and end on the strip boundary or on graphs of other discriminating functions, see figure 11. The graphs decompose $\mathbf{\Omega}$ into regions of similar shapes. It can however happen that two similar shapes correspond to points in different regions. In this case there is no deformation representable in $\mathbf{\Omega}$ that transforms one shape to the other and uses only similar shapes.

Designing in shape space. The initial shape corresponds to the point $P_0 = (0,0)$ in $\mathbf{\Omega}$ and the final shape corresponds to $P_1 = (1,0)$. Every continuous deformation between the two shapes that can be represented

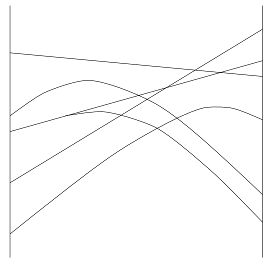

Figure 11: The decomposition of $\mathbf{\Omega}$ into regions of similar shapes. All curves are pieces of lines and parabolas.

in our framework corresponds to a path $p : [0,1] \to \mathbf{\Omega}$ with $p(0) = P_0$ and $p(1) = P_1$. For example the basic deformation described in section 2 corresponds to the straight line segment connecting P_0 with P_1, which is the image of the path $p(u) = (u, 0)$. It may be that more complicated paths give better deformations and we describe how the decomposition of $\mathbf{\Omega}$ is used to find such paths.

An important first step in the rational design of deformations is the computation of *signatures* that are functions from $\mathbf{\Omega}$ to $\mathbb{R}$. An example is the area signature that maps each (t, α^2) to the area of the corresponding body. Strictly speaking that area also depends on the value of the parameter s and we have a signature for each $0 \leq s \leq 1$. Another example is the connectivity of shapes captured by two signatures, $\beta_0, \beta_1 : \mathbf{\Omega} \to \mathbb{R}$, counting components and holes. β_0 and β_1 are independent of s and can be computed directly from the complex, which is homotopy equivalent to the body of the shape [3].

Let $\mathcal{G}$ be the dual graph of the decomposition of $\mathbf{\Omega}$ created by the arrangement of lines and parabolas described above. Let $\beta_0(\nu)$ be the number of components and $\beta_1(\nu)$ be the number of holes of any one shape represented by the region or node ν in $\mathcal{G}$. Let μ_0 and μ_1 be the nodes whose regions contain P_0 and P_1 in their boundaries. A non-degenerate path, $p : [0,1] \to \mathbf{\Omega}$, traces out a sequence of regions and thus translates into a discrete path in $\mathcal{G}$: $\mu_0 = \nu_0, \nu_1, \ldots, \nu_\ell = \mu_1$. Suppose we are interested in a deformation that goes through as few topological changes as possible. The number of such changes that occur along the path p is a sum of absolute differences:

$$\sum_{i=1}^{\ell} |\beta_0(\nu_i) - \beta_0(\nu_{i-1})| + |\beta_1(\nu_i) - \beta_1(\nu_{i-1})|.$$

Think of the term inside the sum as the length of the arc connecting nodes ν_{i-1} and ν_i. The problem of finding a path in $\mathbf{\Omega}$ with minimum topological changes thus reduces to finding a shortest path in $\mathcal{G}$, which can be solved by standard graph algorithms. An improvement of this approach based on the monotonicity of minimizing paths is described in [7].

5 Discussion

This paper describes a method for the automatic deformation of shapes in $\mathbb{R}^2$ and a software tool that implements it.

Algorithms. The basic algorithmic problem raised by the deformation method is the construction of the 1-parameter family of Delaunay complexes $\mathrm{Del}\, A_t$, for $t \in [0, 1]$. As explained in [2], this problem reduces to computing a 4-dimensional convex hull, or equivalently a 3-dimensional (weighted) Delaunay complex. In the latter interpretation the third coordinate is time and $\mathrm{Del}\, A_t$ is the cross-section at $x_3 = t$. $\mathrm{Dsx}\, A_t$ is a subcomplex of $\mathrm{Del}\, A_t$ and the body and skin of the shape are computed from that subcomplex. Our software tool uses the 3-dimensional Delaunay complex algorithm mentioned in [5] and selects subcomplexes as explained in the same reference.

A second interesting algorithmic problem is the construction of the line and parabola arrangement that decomposes the shape space. We implement the incremental algorithm of [4]. The decomposition is typically too fine to be of much use within the user interface. We plan to add a coarse version of the decomposition to the control panel for visualization purposes and to support the manual design of deformation paths. Such coarsenings can be construction with the snap-rounding method described in [6].

Extensions. There are means to impose structure on the shape space other than the arrangement of lines and parabolas described in section 4. Take for example the area signature, $a : \mathbf{\Omega} \to \mathbb{R}$, say for $s = 0.5$. It is continuous and increases with growing α^2. Each level set, $a^{-1}(c)$, is therefore a monotone path connecting a point on the left with a point on the right boundary of $\mathbf{\Omega}$. If P_0 and P_1 are these two points then $a^{-1}(c)$ describes an area preserving deformation between the two corresponding shapes.

Any application to image morphing will almost surely require a way to carry color and pattern along with the shape through the deformation. Maybe one of the background structures, such as the mixed complex that decomposes the body and moves with it, can be used for that purpose.

Applications in data compression and databases for shapes will find the restriction to *two* base shapes unreasonably limiting. As explained in [2], the mathematical framework for deformation readily extends to any fixed number of base shapes. However, all algorithmic problems get significantly harder as the dimension of the shape space increases.

References

[1] J. Blinn. A generalization of algebraic surface drawing. *ACM Trans. Graphics* **2** (1980), 235–256.

[2] H.-L. Cheng, H. Edelsbrunner and P. Fu. Shape space from deformation. Report rgi-tech-011, Raindrop Geomagic, Champaign, Illinois, 1998.

[3] H. Edelsbrunner. Deformable smooth surface design. *Discrete Comput. Geom.*, to appear.

[4] H. Edelsbrunner, L. J. Guibas, J. Pach, R. Pollack, R. Seidel and M. Sharir. Arrangements of curves in the plane-topology, combinatorics and algorithms. *Theoret. Comput. Sci.* **92** (1992), 319–336.

[5] H. Edelsbrunner and E. P. Mücke. Three-dimensional alpha shapes. *ACM Trans. Graphics* **13** (1994), 43–72.

[6] L. J. Guibas and D. Marimont. Rounding arrangements dynamically. *In* "Proc. 11th Ann. Sympos. Comput. Geom. 1995", 190-199.

[7] K. P. Lam. Two-dimensional geometric morphing. Master thesis, Dept. Comput. Sci., Hong Kong University of Science and Technology, 1996.

[8] S. Y. Lee, K. Y. Chwa, J. Hahn and S. Y. Shin. Image morphing using deformation techniques. *J. Visualization Comput. Animation* **7** (1996), 3–23.

[9] S. M. Seitz and C. R. Dyer. View morphing. *Computer Graphics* **50** (1996), 21–30.

[10] G. Wolberg. Recent advances in image morphing. *In* "Proc. Computer Graphics Internat. 1996", 64–71.

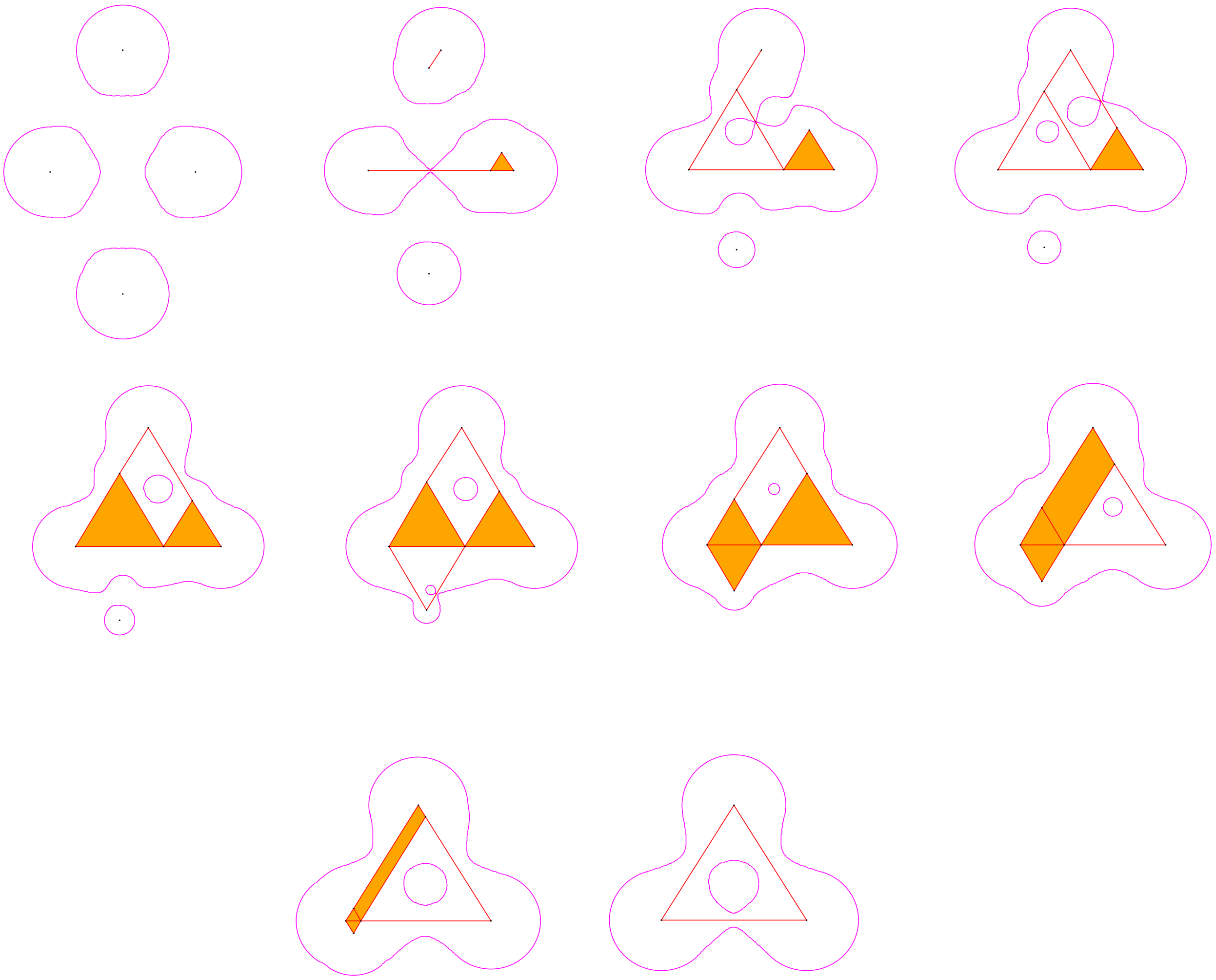

Figure 5: Ten snapshots of a deformation with complex and skin displayed. The parameter s for all shapes is 0.5. The set of disks that generates the complex and the skin in the fifth snapshot is the same as in figures 2, 3, 4.

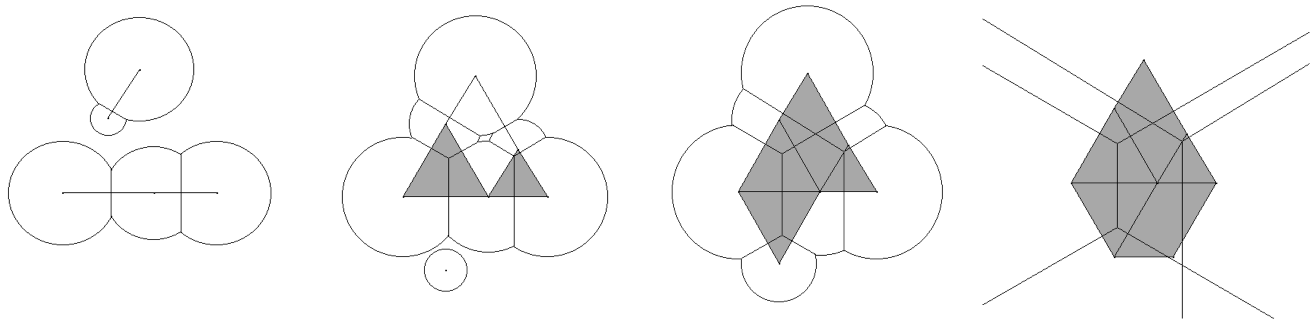

Figure 6: Decomposed disk union and α-complex for four values of α. In the second example we have $\alpha = 0$ and therefore the same complex as in figure 3. In the fourth example we have α sufficiently large so that the α-complex is the Delaunay complex.

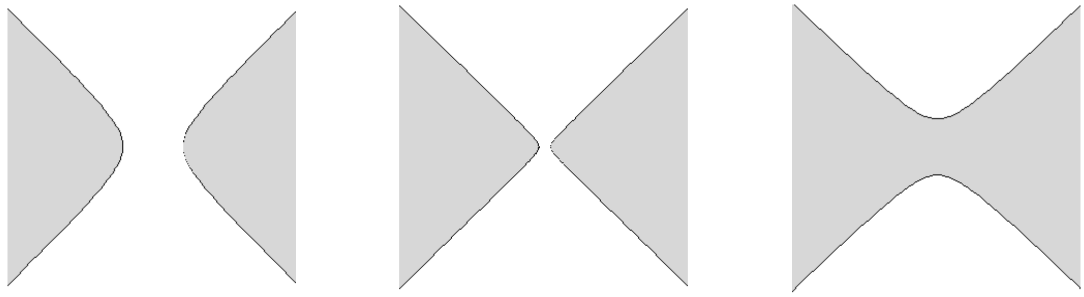

Figure 9: From left to right the sequence illustrates the creation of a bridge through flipping a hyperbola. From right to left it illustrates the removal of that bridge.

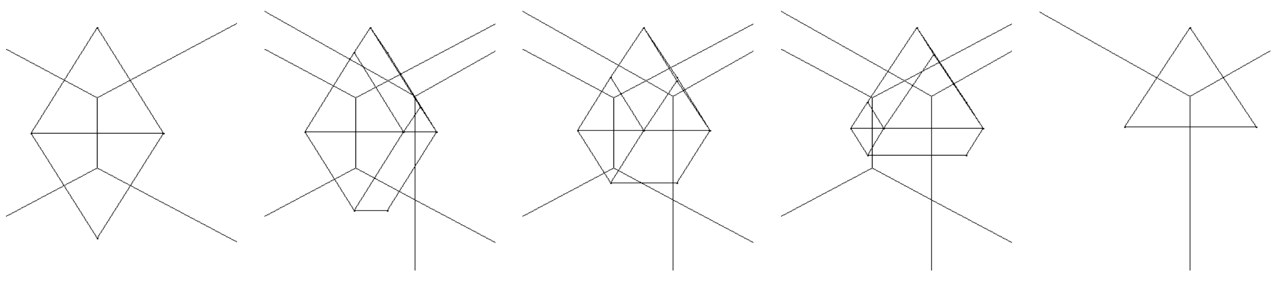

Figure 10: The Vornonoi and Delaunay complexes at times $t = 0, 0.25, 0.5, 0.75, 1$ during the deformation.